Supporting Information

Cu-modified $CoSe_2$ nanoarrays for efficient electrocatalytic nitrite reduction to ammonia

Jiawen Wang, [a] Man Qiao, [a] Shuaiyou Chen, [b] Xue Lu, [c] Jiahui Shen, *[b] Dongsheng Geng [a] and Dongdong Zhu*[a]

[a] School of Chemistry and Materials Science, Jiangsu Key Laboratory of New Energy Devices and Interface Science, Nanjing University of Information Science and Technology, Nanjing 210044, China. E-mail: dd.zhu@nuist.edu.cn

[b] Key Laboratory of Urban Rail Transit Intelligent Operation and Maintenance Technology & Equipment of Zhejiang Province, College of Engineering, Zhejiang Normal University, Jinhua 321004, China. E-mail: shenjh@zjnu.edu.cn

[c] College of Science, Nanjing Forestry University, Nanjing 210037, China.

1 Experimental section

1.1 Materials

Sodium citrate ($C_6H5O_7Na_3$), salicylic acid ($C_7H_6O_3$), Se powder, sodium hydroxide (NaOH) and sodium nitroferricyanide dihydrate ($C_5FeN_6Na_2O \cdot 2H_2O$) were purchased from Aladdin Ltd. (Shanghai, China). Potassium hydroxide (KOH), ammonium chloride (NH_4Cl), and sodium hypochlorite (NaClO) were purchased from Macklin Inc. (Shanghai, China). Cobalt(II) nitrate hexahydrate ($Co(NO_3)_2 \cdot 6H_2O$), ethanol absolute (C_2H_5OH), boric acid (H_3BO_3), copper(II) sulfate pentahydrate ($CuSO_4 \cdot 5H_2O$), sodium pyrophosphate tetrabasic decahydrate ($Na_4P_2O_7 \cdot 10H_2O$), sodium borohydride ($NaBH_4$), potassium nitrite (KNO_2), and hydrochloric acid (HCl) were purchased from China National Pharmaceutical Group Corp. (China). All reagents in this work were used without further purification. Ultrapure water (Millipore Milli-Q grade) with a resistivity of 18.25 MΩ was used in all experiments.

1.2 Preparation of Cu-$CoSe_2$

A piece of Ni Foam (NF, 2 cm × 3 cm) was ultrasonicated in 2.0 M hydrochloric acid, ethanol absolute, and Milli-Q water for 8 min, respectively. Firstly, 2.0 mmol of $NaBH_4$, 1 mmol of Se powder, 1 mmol $Co(NO_3)_2 \cdot 6H_2O$, 1.5 mL of Milli-Q water and 30 mL ethanol were mixed together to form a transparent solution by magnetic stirring. Then the solution was transferred to a 50 mL Teflon-lined stainless-steel autoclave in which a piece of Ni foam was immersed into it. The autoclave was sealed and maintained at 140°C for 8 hours in an electric oven. After the autoclave cooled down to room temperature, the $CoSe_2$/NF was taken out and washed with water and ethanol several times, followed by drying at 60°C for 12 h. Secondly, $CoSe_2$ was annealed in nitrogen at 350°C for 2 hours. Finally, Cu was introduced onto the $CoSe_2$ nanoarrays via an electrodeposition method. The electrodeposition was conducted in a standard three-electrode system, where the $CoSe_2$ electrode on NF served as the working electrode, with a Hg/HgO electrode and a platinum sheet electrode acting as the reference electrode and counter electrode, respectively. The electrolyte was prepared by dissolving 22.0 mmol of $Na_4P_2O_7 \cdot 10H_2O$, 22.0 mmol of NH_4Cl, and 0.25 mmol of

$CuSO_4 \cdot 5H_2O$ in 50 mL of 0.1 M boric acid solution. Cu deposition was performed for 5 min at a constant current density of 0.5 A cm^{-2}. The resulting electrode was rinsed with deionized water and dried overnight in a vacuum drying oven to obtain Cu-$CoSe_2$. For comparison, $CoSe_2$ was synthesized similar to that of Cu-$CoSe_2$ without the Cu electrodeposition step. Cu was prepared *via* direct electrodeposition on Ni foam.

1.3 Characterizations

The X-ray diffraction (XRD) patterns of the samples were obtained on Smart Lab/3kW with Cu Kα radiation. The morphology of the samples was characterized by field emission scanning electron microscopy (FESEM, Zeiss Gemini SEM 300) equipped with an energy dispersive spectrometer (EDS) and transmission electron microscopy (TEM, JEOL JEM-2100F). X-ray photoelectron spectroscopy (XPS) measurements were carried out on an ESCALab250 using Al Kα radiation, and the working voltage is 12.5 kV. The binding energy was calibrated to the C 1s peak of 284.8 eV.

1.4 Electrochemical measurements

All electrochemical measurements reported in this study were performed on a CHI 760E electrochemical workstation (Chenhua, Shanghai). The electrocatalytic performance of the obtained catalysts was evaluated by using a two-chamber H-type cell with a three-electrode system in which the cathode chamber was separated from the anode chamber through a cation exchange membrane (Nafion 117). The prepared electrodes were used as the cathode, while Pt sheet and Hg/HgO electrode served as the counter and reference electrodes, respectively, and 1.0 M KOH solution (40 mL) containing 0.1 M KNO_2 was used as electrolyte. The linear sweep voltammetry (LSV) was performed at a scan rate of 2 mV s^{-1}. All potentials were recorded against the reversible hydrogen electrode (RHE), and 90%iR correction was applied for the presented results. The potentiostatic test was carried out at different potentials for 1 hour with a stirring rate of 1000 rpm.

1.5 Detection of ammonia

The NH_3 concentration was determined by indophenol blue spectrophotometry. Under alkaline conditions, ammonia nitrogen (NH_3/NH_4^+) reacts with NaClO and phenolic compounds (phenol or salicylic acid) to produce the blue color indophenol blue in the presence of a sodium nitroferricyanide dihydrate catalyst. Firstly, 2.5 g of sodium citrate and 2.5 g of salicylic acid were dissolved in 50.0 mL of 1.0 M NaOH to prepare the colorant, noted as Reagent A. Reagent B was 0.05 M NaClO. Dissolve 0.2 g of $C_5FeN_6Na_2O \cdot 2H_2O$ in 20 mL of ultrapure water to prepare the catalyst, noted as Reagent C. Secondly, the quantification process is as follows: take out a certain amount of electrolyte and dilute it to the detection range. Then take 2 mL of the diluted solution and add 2.0 mL of reagent A, 1.0 mL of reagent B and 0.2 mL of reagent C in turn, shake well to mix, and leave it for 2 hours away from light. Next, the UV-Vis absorbance was measured at a wavelength of 655 nm. The concentration-absorbance curve was calibrated using the standard NH_4Cl solution with concentrations of 0, 0.50, 1.00, 1.50, 2.00, and 2.50 ppm of 1.0 M KOH solution. Then the concentration of NH_3 product was calculated according to the absorbance and standard curve.

1.6 Calculation of faradaic efficiency (FE) and NH_3 yield

NH_3 FE = $(6 \times F \times V \times C \times A) / (M_{NH_3} \times Q) \times 100\%$

NH_3 yield = $(C \times V \times A) / (M_{NH_3} \times S \times t)$

Where F is the Faraday constant (96485 C mol^{-1}), V is the volume of electrolyte in the H-cell cathode chamber (40 mL), C is the measured concentration of the diluted product, A is the dilution factor, M_{NH_3} is the molar mass of NH_3, Q is the total quantity of applied electricity, S is the loaded area of catalyst (0.5 cm × 0.5 cm), t is the electrolysis time (1 hour).

1.7 DFT Calculation

All spin-polarized density functional theory (DFT) calculations were performed using the Vienna Ab Initio Simulation Package (VASP)[1,2] within the generalized gradient approximation (GGA) and the Perdew–Burke–Ernzerhof (PBE)[3] functional. The ion–electron interactions were described by the projector augmented-wave (PAW) method[4,5], and the valence electrons were expanded in a plane-wave basis set with a kinetic energy cutoff of 400 eV. Gaussian smearing with a width of 0.05 eV was applied to treat partial occupancies of the Kohn–Sham orbitals. Dispersion corrections were included using Grimme's DFT-D3 scheme[6]. A $CoSe_2$(101) surface model was constructed with p(2×2) periodicity in the x- and y-directions and three stoichiometric layers along the z-direction. A vacuum layer of 15 Å was added to avoid spurious interactions between periodic images. The resulting orthogonal supercell contains 24 Co and 48 Se atoms. During structural relaxation, the Brillouin zone was sampled with a 2×1×1 k-point mesh. The top stoichiometric layer was allowed to relax fully, while the bottom two layers were kept fixed. The doping model was built with a Cu_4 cluster.

1.8 Assembly of the Zn-NO_2^- battery and electrochemical test

The Zn-NO_2^- battery measurements were carried out in a customized H-type glass cell which contains 40 mL cathodic electrolyte (1.0 M KOH + 0.1 M KNO_2) and 40 mL anodic electrolyte (1.0 M KOH) separated by a Nafion 117 membrane at room temperature. The NF supported Cu-$CoSe_2$ (1 × 1 cm^2) and Zn plate (2 × 1.5 cm^2) were used as the cathode and anode for Zn-NO_2^- battery, respectively. Discharge polarization curves and discharge tests at different current densities were obtained by testing on CHI 760E electrochemical workstation. Constant current charge-discharge of Zn-NO_2^- battery was performed on CS2350M electrochemical workstation (Cortest Instruments, China). The power density (P) of the Zn-NO_2^- battery was determined by using following equation: $P = I \times V$, where I and V are the discharge current density and corresponding voltage, respectively.

1.9 NO_2RR product collection from Zn-NO_2^- battery

First, the Zn-NO_2^- battery was discharged at a current density of 20 mA cm^{-2} for 12 h, and the electrolyte from the NO_2^- side was collected. NH_3 was then recovered *via* an argon stripping method coupled with an acid trap. Specifically, 40 mL of the collected electrolyte was sealed in a flask and heated at 50 °C, while a 150 mL min^{-1} argon flow was passed through the solution for 12 h to strip the NH_3. The outlet gas stream was directed into 40 mL of 0.3 M HCl to trap the NH_3 product. The resulting acid solution containing the captured NH_3 was dried using a rotary evaporator, and the collected powder sample was further dried overnight in an oven at 60 °C to yield NH_4Cl (s).

2 Supplementary Figures and Tables

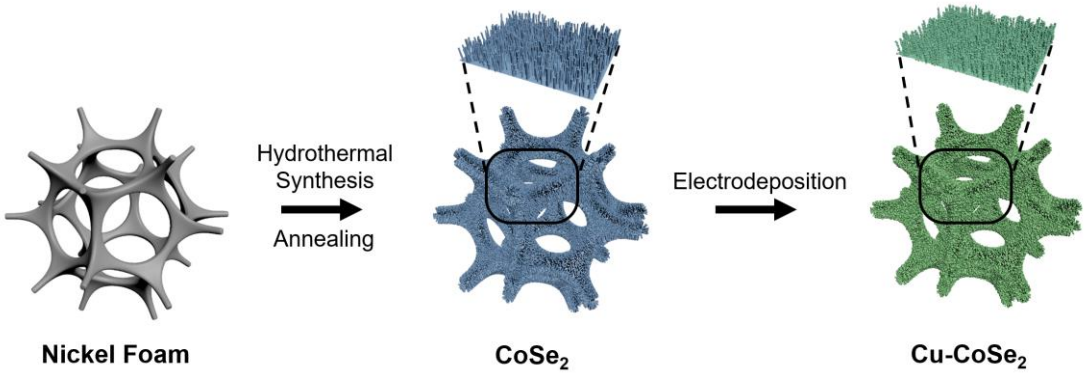

Figure S1. Schematic illustration of the synthesis process for Cu-$CoSe_2$ on Ni foam.

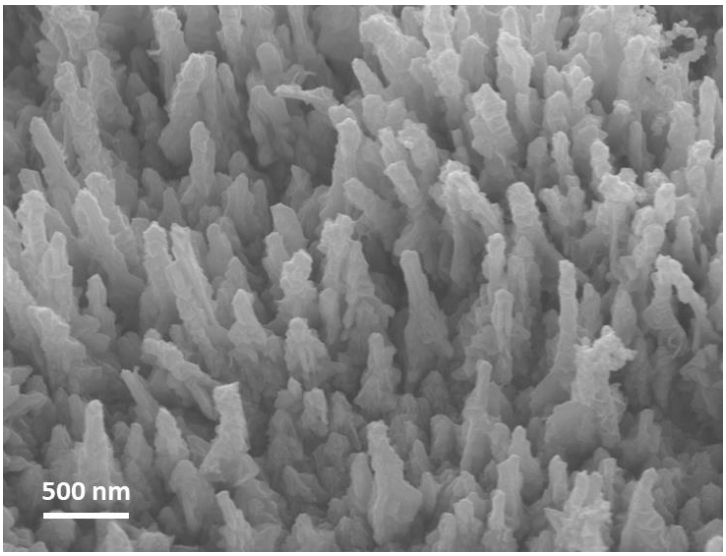

Figure S2. SEM image of $CoSe_2$.

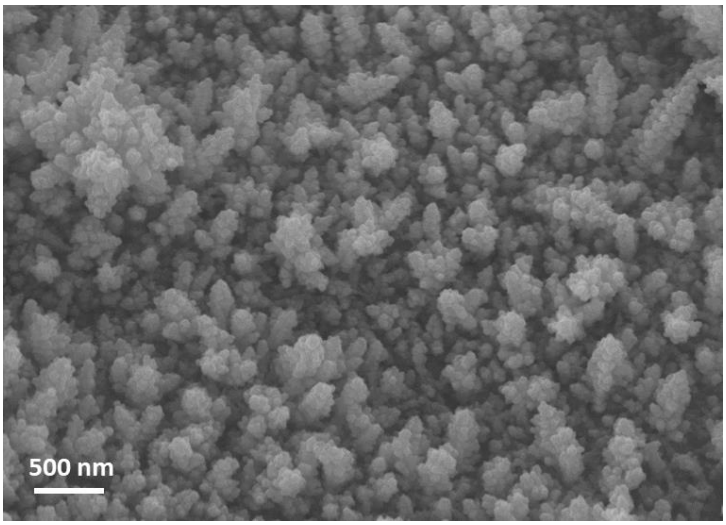

Figure S3. SEM image of Cu-$CoSe_2$.

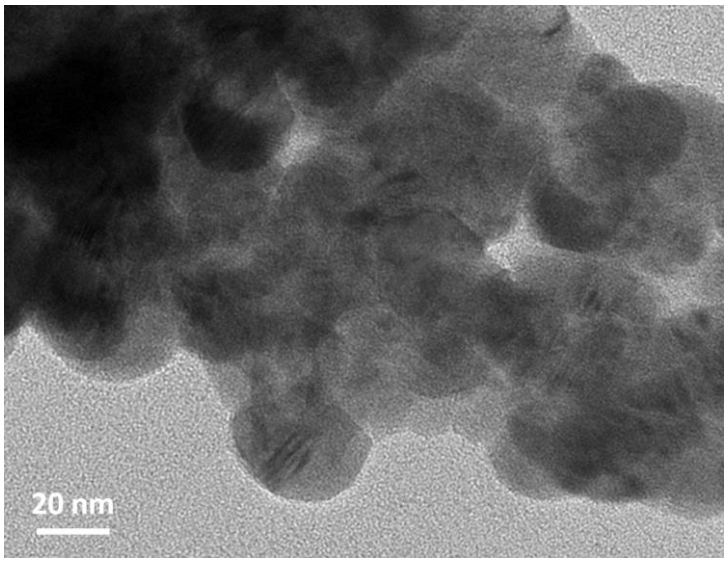

Figure S4. TEM image of Cu-$CoSe_2$ with different resolution.

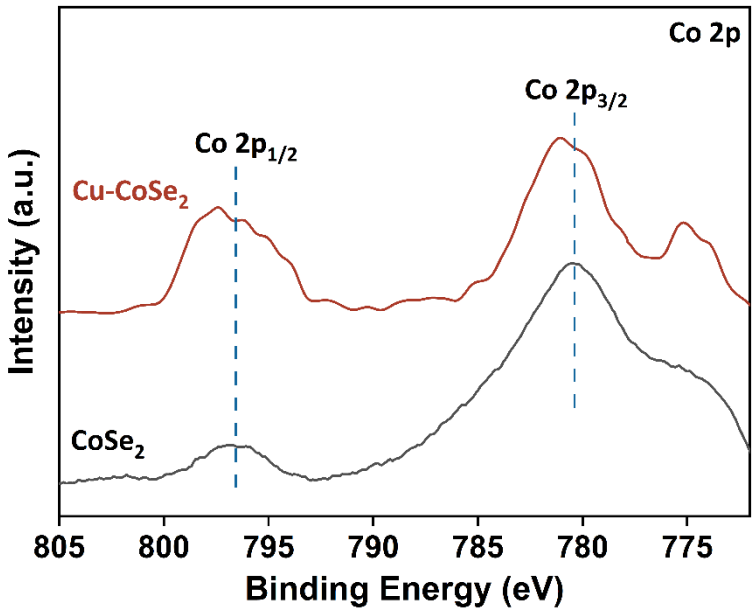

Figure S5. XPS Co 2p spectra of Cu-$CoSe_2$ and $CoSe_2$.

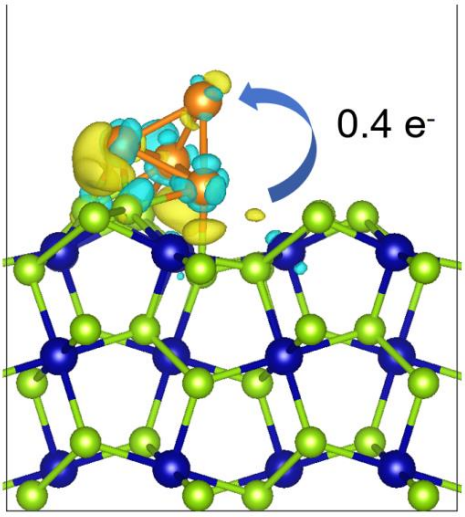

Figure S6. The charge density difference in Cu-$CoSe_2$, yellow represents electron accumulation and cyan represents electron depletion. Orange atom: Cu, blue atom: Co, green atom: Se.

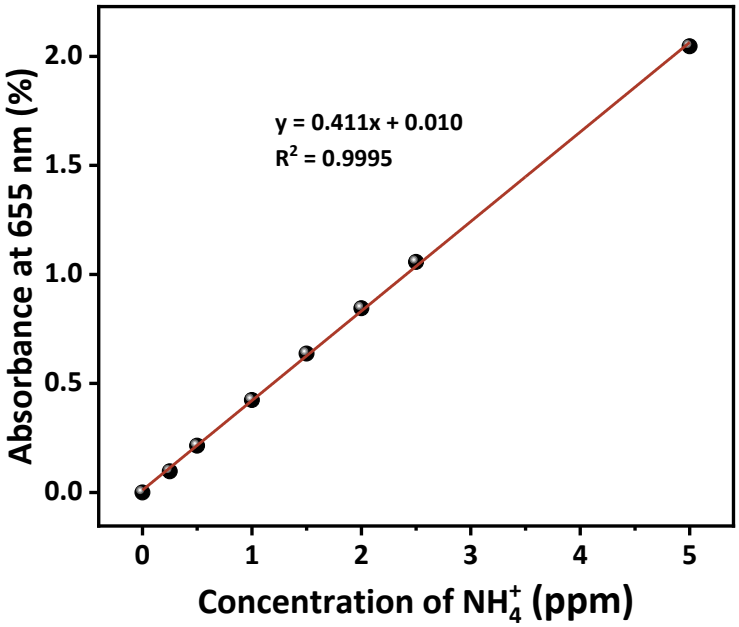

Figure S7. The concentration-absorbance calibration curve for NH_4^+.

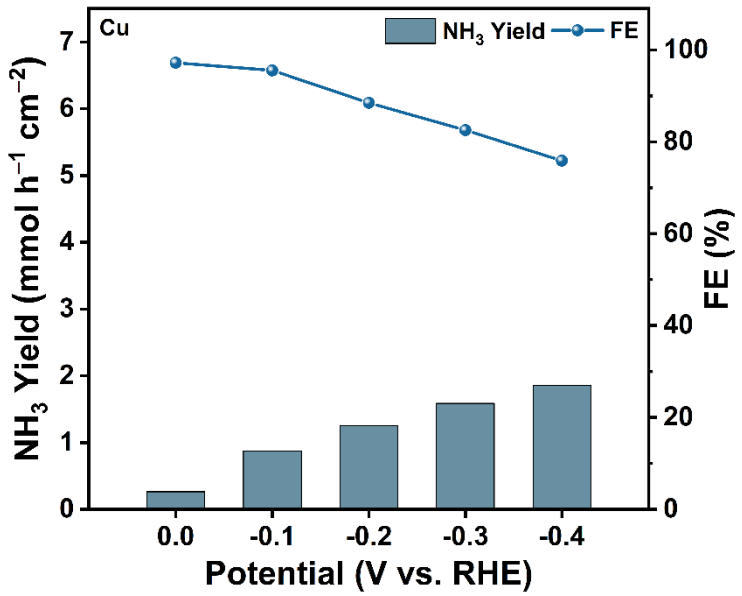

Figure S8. NH_3 yields and FEs of Cu tested at different applied potentials for 1 hour in 1.0 M KOH with 0.1 M NO_2^-.

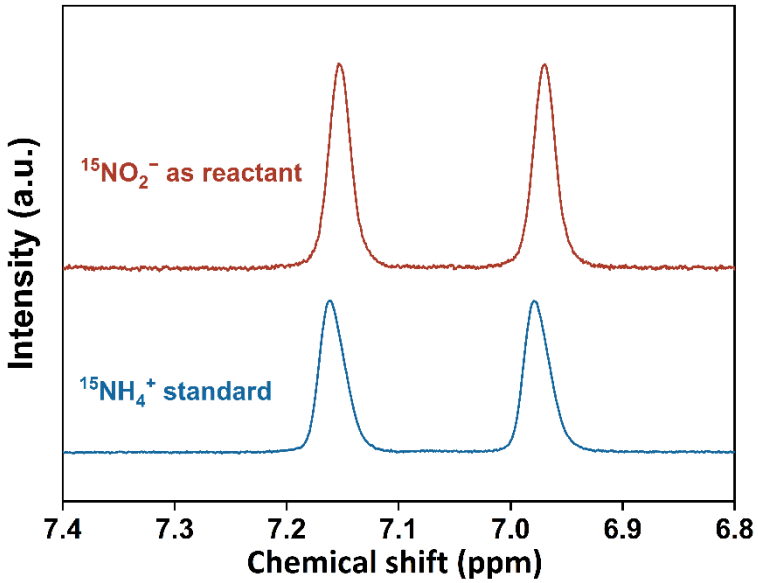

Figure S9. ^{1}H-NMR spectra of the electrolyte obtained after NO_2RR using $K^{15}NO_2$ as the nitrogen source, and the standard $^{15}NH_4Cl$ electrolyte.

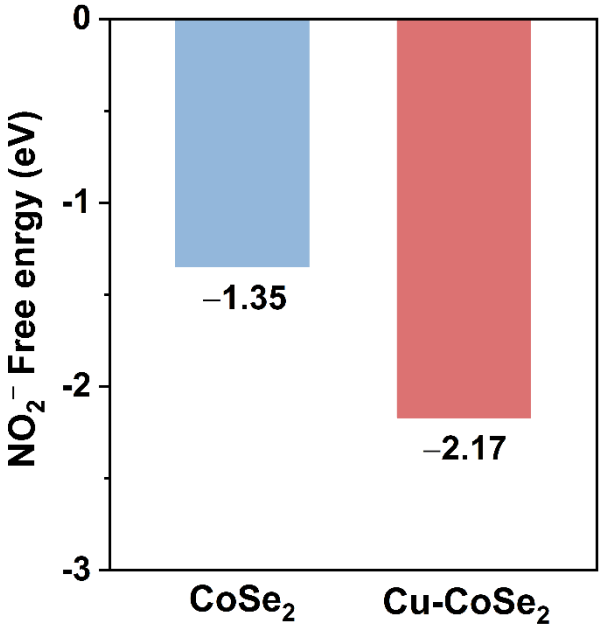

Figure S10. The NO_2^- adsorption energy on $CoSe_2$ and Cu-$CoSe_2$.

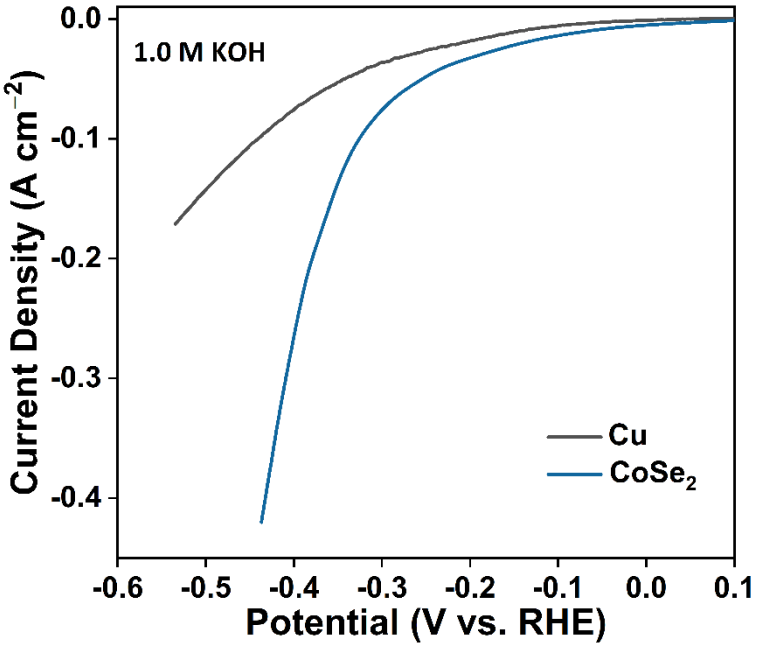

Figure S11. LSV curves of Cu and $CoSe_2$ samples tested in 1.0 M KOH.

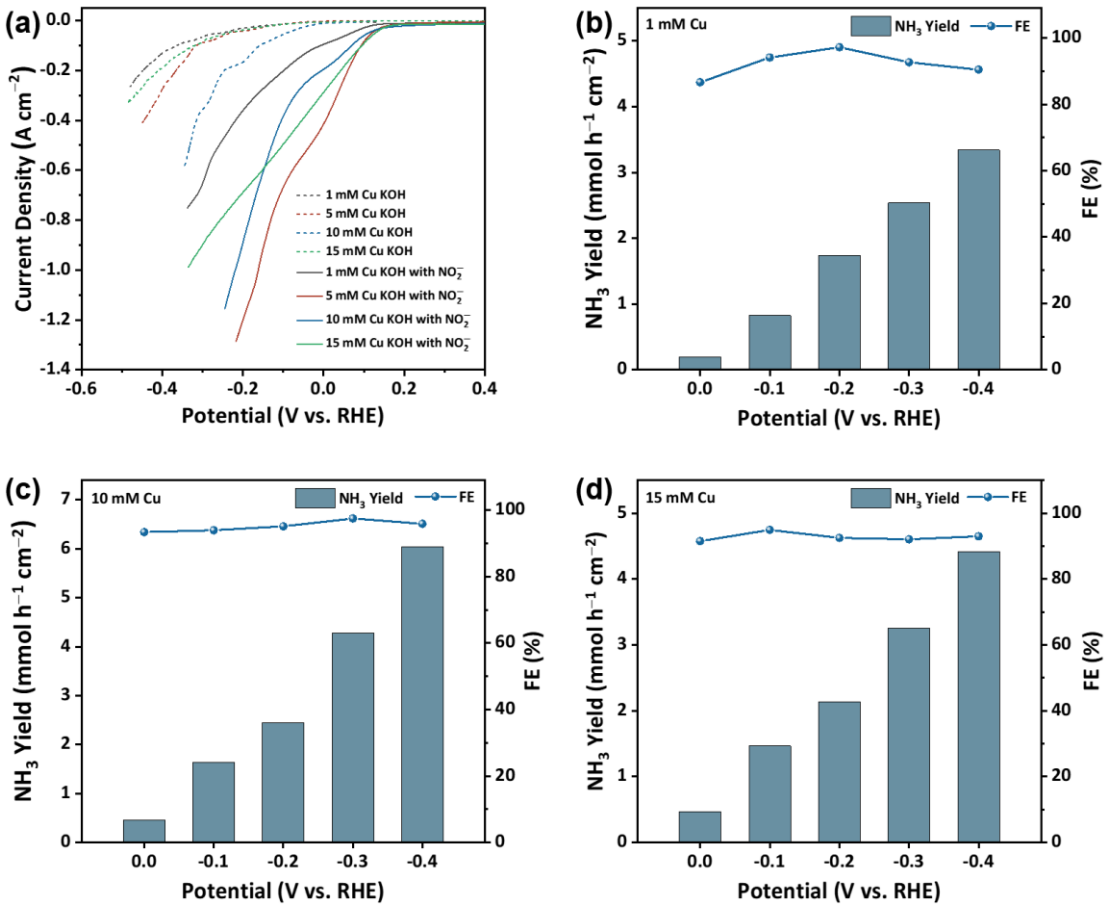

Figure S12. In 1.0 M KOH with 0.1 M NO_2^-, NO_2RR performance of Cu-$CoSe_2$ samples prepared with different Cu content in the electrodeposition solution. (a) LSV curves of Cu-$CoSe_2$ samples, (b) NH_3 yields and FEs of Cu-$CoSe_2$ sample prepared with 1 mM $CuSO_4$, (c) NH_3 yields and FEs of Cu-$CoSe_2$ sample prepared with 10 mM $CuSO_4$, and (d) NH_3 yields and FEs of Cu-$CoSe_2$ sample prepared with 15 mM $CuSO_4$.

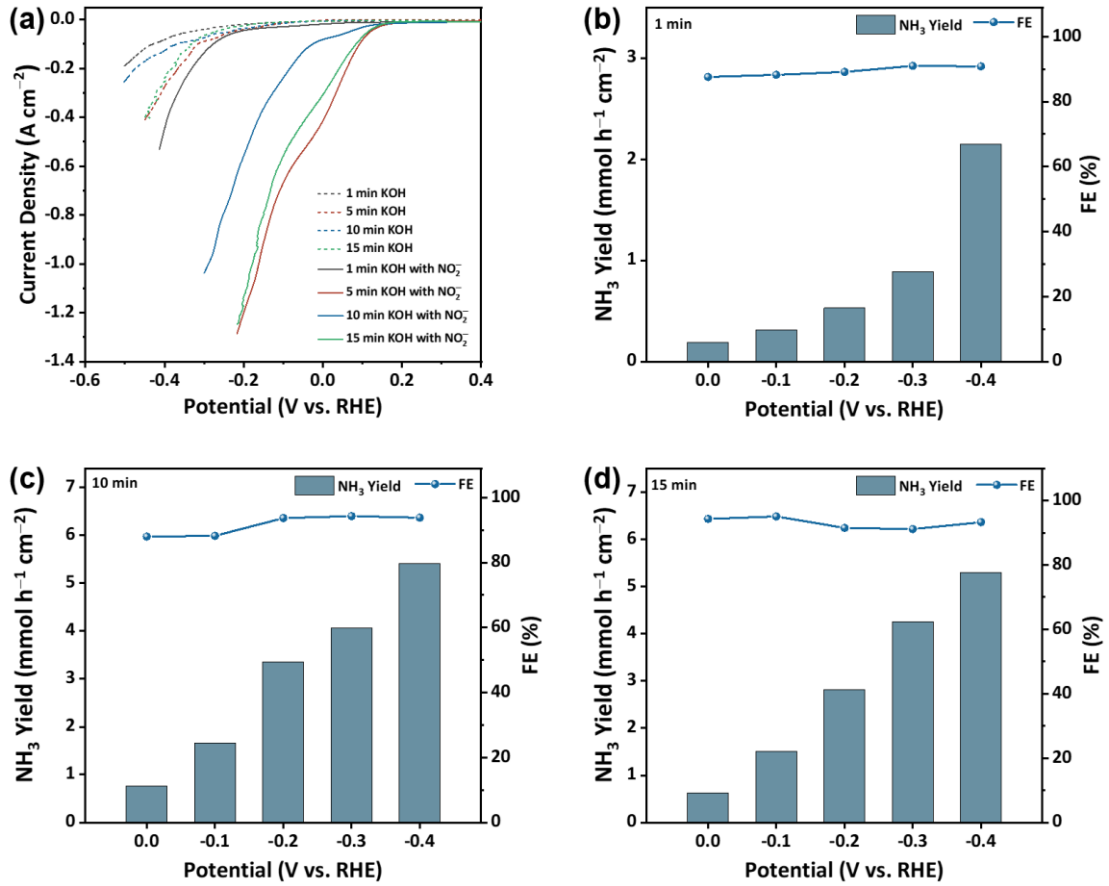

Figure S13. In 1.0 M KOH with 0.1 M NO_2^-, NO_2RR performance of Cu-$CoSe_2$ samples prepared with different electrodeposition time. (a) LSV curves of Cu-$CoSe_2$ samples, (b) NH_3 yields and FEs of Cu-$CoSe_2$ sample prepared with 1 min, (c) NH_3 yields and FEs of Cu-$CoSe_2$ sample prepared with 10 min, and (d) NH_3 yields and FEs of Cu-$CoSe_2$ sample prepared with 15 min.

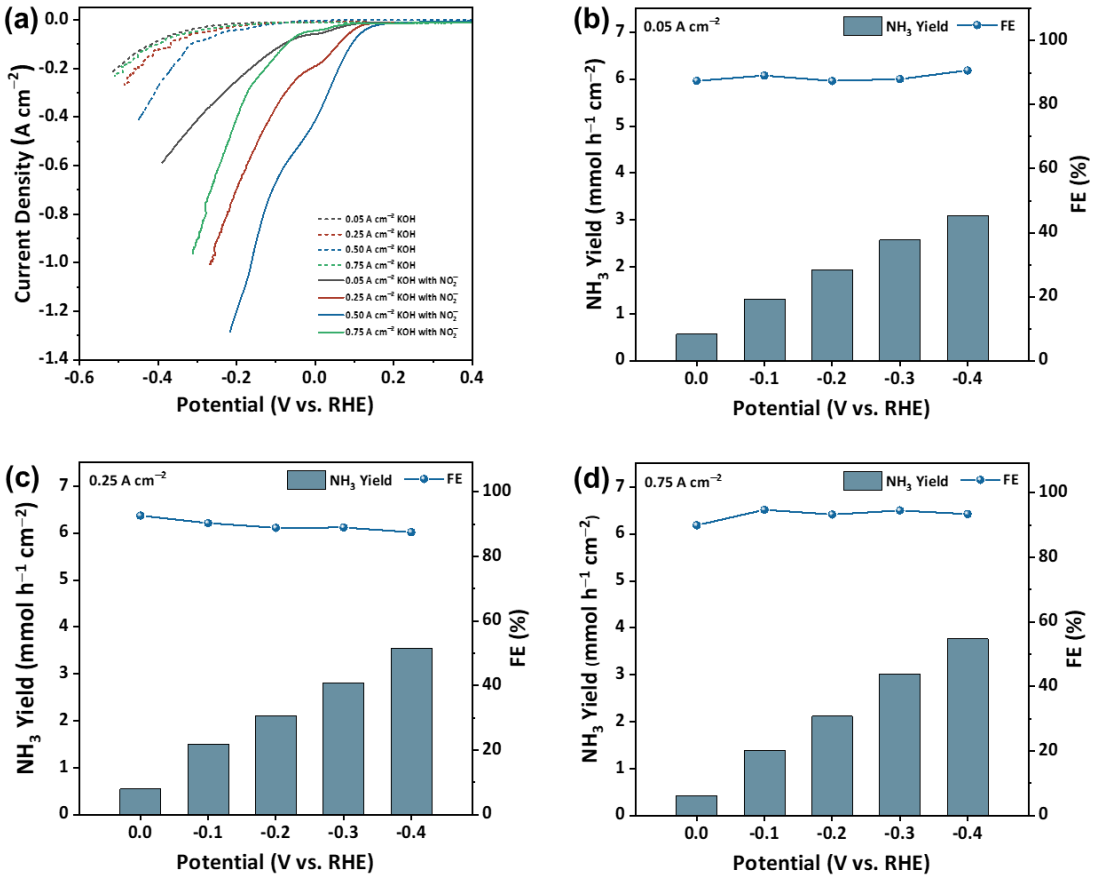

Figure S14. In 1.0 M KOH with 0.1 M NO_2^-, NO_2RR performance of Cu-$CoSe_2$ samples prepared with different electrodeposition current density. (a) LSV curves of Cu-$CoSe_2$ samples, (b) NH_3 yields and FEs of Cu-$CoSe_2$ sample prepared with 0.05 A cm^{-2}, (c) NH_3 yields and FEs of Cu-$CoSe_2$ sample prepared with 0.25 A cm^{-2}, and (d) NH_3 yields and FEs of Cu-$CoSe_2$ sample prepared with 0.75 A cm^{-2}.

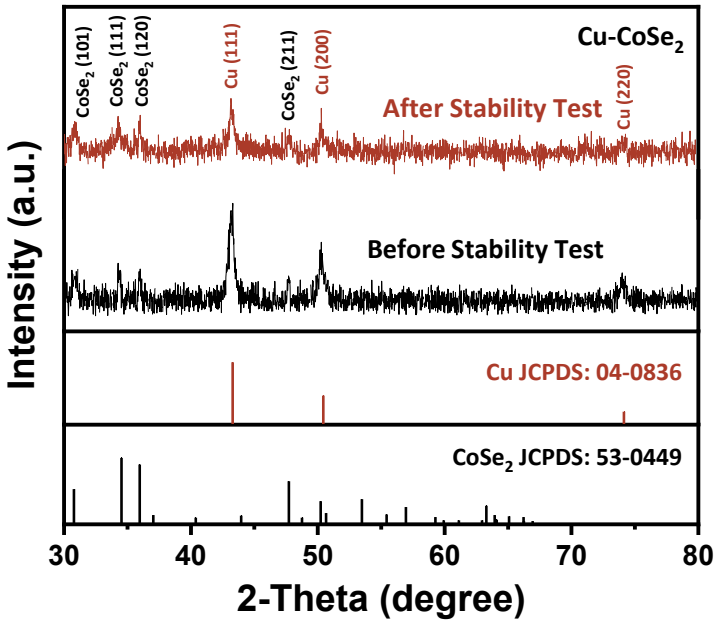

Figure S15. XRD patterns of Cu-$CoSe_2$ tested before and after NO_2RR cycling test.

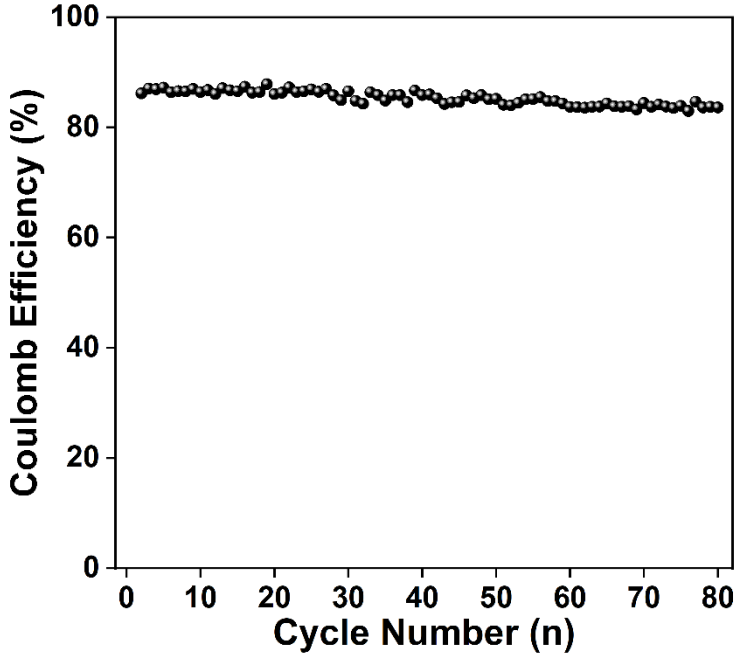

Figure S16. The coulombic efficiency of the Zn-NO_2^- battery for 80 cycles.

Table S1. Summary of the electrochemical NO_2RR performance of some representative electrocatalysts in alkaline electrolytes.

Catalyst	**Potential (V vs. RHE)**	**NH_3 Yield (mmol h^{-1} cm^{-2})**	**FE (%)**	**Electrolyte**	**Ref.**
Cu-$CoSe_2$	−0.3	4.792	98.66	1.0 M KOH + 0.1 M NO_2^-	This Work
$Cu_{0.8}Zn_{0.2}NCN$	−0.5	1.294	87.8	1.0 M KOH + 0.5 M NO_2^-	7
CuO/Co_3O_4	−0.4	1.853	97.6	1.0 M NaOH + 0.1 M NO_2^-	8
Co_3S_4	−0.3	1.129	96.9	1.0 M NaOH + 0.1 M NO_2^-	9
RhRu-$MoSe_{2-x}O_y$	−0.2	4.636	93.0	0.5 M KOH + 0.5 M NO_2^-	10
Cu_3P@TiO_2	−0.7	1.583	97.1	0.1 M NaOH + 0.1 M NO_2^-	11
Pd/MBene	−0.3	0.994	89.0	0.1 M NaOH + 0.1 M NO_2^-	12
Ru-TiO_2	−0.5	1.560	98.9	0.1 M NaOH + 0.1 M NO_2^-	13
Ni@WO_2	−0.4	1.056	94.6	0.1 M NaOH + 0.1 M NO_2^-	14
Cu_2O/NiO	−0.4	0.682	95.7	0.1 M NaOH + 0.1 M NO_2^-	15
single-atom alloy CuZn	−0.8	0.167	96.1	0.2 M $KHCO_3$ + 10 mM NO_2^-	16

References

1 G. Kresse, J. Furthmüller, *Comput. Mater. Sci.* 1996, **6**, 15−50.

2 G. Kresse, J. Furthmüller, *Phys. Rev. B* 1996, **54**, 11169−11186.

3 J. P. Perdew, K. Burke, M. Ernzerhof, P*hys. Rev. Lett.* 1996, **77**, 3865−3868.

4 G. Kresse, D. Joubert, *Phys. Rev. B* 1999, **59**, 1758-1775.

5 P. E. Blöchl, *Phys. Rev. B* 1994, **50**, 17953−17979.

6 S. Grimme, J. Antony, S. Ehrlich, H. Krieg, *J. Chem. Phys.* 2010, **132**, 154104.

7 J. J. Wang, H. T. D. Bui, X. Wang, Z. Lv, H. Hu, S. Kong, Z. Wang, L. Liu, W. Chen, H. Bi, M. Yang, T. Brinck, J. Wang and F. Huang, *J. Am. Chem. Soc.*, 2025, **147**, 8012–8023.

8 Z. Niu, S. Fan, X. Li and G. Chen, *Adv. Energy Mater.*, 2024, **14**, 2303515.

9 C. Zhang, X. Wang, J. Jiang, J. Zhang, A. Liu and L. Ai, *Appl. Catal. B Environ. Energy*, 2025, **365**, 124991.

10 Z. Luo, L. Shi, Y. Qian, Z. Yang, J. Li, L. Zhang, Q. Zhang, C. He and X. Ren, *Adv. Funct. Mater.*, 2025, e13568.

11 Z. Cai, D. Zhao, X. Fan, L. Zhang, J. Liang, Z. Li, J. Li, Y. Luo, D. Zheng, Y. Wang, T. Li, H. Yan, B. Ying, S. Sun, A. A. Alshehri, H. Yan, J. Xu, Q. Kong and X. Sun, *Small*, 2023, **19**, 2300620.

12 J. Zhang, Q. Zeng, X. Wang, L. Ai, C. Zhang, A. Liu and J. Jiang, *Adv. Funct. Mater.*, 2025, **35**, 2504632.

13 Y. Ren, Q. Zhou, J. Li, X. He, X. Fan, Y. Fu, X. Fang, Z. Cai, S. Sun, M. S. Hamdy, J. Zhang, F. Gong, Y. Liu and X. Sun, *J. Colloid Interface Sci.*, 2023, **645**, 806–812.

14 H. Qiu, Q. Chen, J. Zhang, X. An, Q. Liu, L. Xie, W. Yao and Q. Kong, *J. Mater. Chem. A*, 2025, **13**, 1738–1745.

15 Y. Feng, X. Lv, H. Wang, H. Wang, F. Yan, L. Wang, H. Wang, J.-T. Ren and Z.-Y. Yuan, *Adv. Funct. Mater.*, 2025, **35**, 2425687.

16 J. Lan, Z. Wang, C. Kao, Y.-R. Lu, F. Xie and Y. Tan, *Nat. Commun.*, 2024, **15**, 10173.